

Journal of
Mechanics of
Materials and Structures

**FINITE STRAIN MICROMECHANICAL ANALYSIS FOR
THERMOELASTOPLASTIC MULTIPHASE MATERIALS**

Jacob Aboudi

Volume 3, N° 5

May 2008



mathematical sciences publishers

FINITE STRAIN MICROMECHANICAL ANALYSIS FOR THERMOELASTOPLASTIC MULTIPHASE MATERIALS

JACOB ABOUDI

A micromechanical model that is based on the homogenization technique for periodic composites is developed for the prediction of the response of multiphase materials undergoing large deformations. Every one of the constituents is supposed to be either a rate-independent thermoelastoplastic material or a thermoelastic one, both of which are formulated in the framework of finite strains. Hyperelastic constituents are obtained as a special case. The resulting macroscopic (global) constitutive equations of the composite involve the instantaneous mechanical and thermal tangent tensors. The reliability of the prediction is examined by comparisons with the composite cylinder assemblage model, which is formulated for a finite strain rate-independent thermoplasticity and is valid under axisymmetric loading. Applications are given for a system of a rubber-like matrix reinforced by metallic fibers. In addition, the behavior of rate-independent elastoplastic laminated materials undergoing large deformations and subjected to in-plane loading is investigated. Finally, the response of an elastoplastic auxetic metallic material, which is capable of generating a negative Poisson's ratio at any stage of a finite strain loading is examined by employing the proposed micromechanical model.

1. Introduction

Finite strain inelastic anisotropic constitutive relations have been proposed for the modeling of the mechanical behavior of biological tissues. To this end, [Tanaka and Yamada \[1990\]](#) and [Tanaka et al. \[1996\]](#) combined the deformation due to an elastic transversely isotropic energy function with a viscoplastic deformation part in order to establish inelastic anisotropic constitutive relations for the finite strain modeling of the behavior of arteries and ventricular walls. More recently, [Gasser and Holzapfel \[2002\]](#) proposed a rate-independent finite strain elastoplastic anisotropic constitutive model for biological fiber-reinforced composites. The elastic part of the deformation is described by an anisotropic energy function, whereas the inelastic part is described by plastic slip on given planes which is the concept of slip systems used in rate-independent crystal plasticity. It should be noted that, in general, the modeling of the large deformations of hyperelastic anisotropic materials requires a formulation of a strain-energy function that consists of a dependence on five invariants for transversely isotropic behavior. For orthotropic materials a dependence on seven invariants is necessary, while for composites with two families of fibers the number of invariants is eight [[Spencer 1971; 1984; Holzapfel 2000](#)]. Thus, it is quite obvious that, in general, the establishment of such energy functions is very complicated.

A micromechanical analysis that is based on the properties of the constituents and the detailed representation of their interaction forms an alternative approach for the finite strain inelastic anisotropic

Keywords: periodic unidirectional composites, finite Plasticity, large deformations, composite materials, high-fidelity generalized method of cells.

modeling of materials and biological tissues. Such an approach was followed by [van der Sluis et al. \[2001\]](#) where the homogenization method for periodic composites has been employed to analyze a composite that consists of a polycarbonate elastic-viscoplastic matrix reinforced by elastic particles. The elastic-viscoplastic matrix is modeled as a hyperelastic isotropic material in the elastic region, whereas Perzyna's viscoplasticity [\[1966\]](#) is used to characterize the inelastic part. The additive decomposition of the rate of deformation tensor is used in conjunction with the objective Truesdell stress rate. The rubber inclusions are modeled by a hyperelastic compressible isotropic neo-Hookean constitutive law. Finally, the finite element procedure is employed to solve the governing equations. Finite strain viscoplastic composites were also modeled by a micromechanical analysis referred to as *high-fidelity generalized method of cells* (HFGMC) which is based on the homogenization technique for periodic composites [\[Aboudi 2004a; 2004b\]](#). To this end, the monolithic inelastic matrix was modeled by the elastic-viscoplastic constitutive relations with isotropic and directional hardening of [Rubin \[1987\]](#) (in which, in particular, the stress is not characterized by a hypoelastic equations so that no special rates of stress need to be considered).

In the present investigation, we offer to generalize the HFGMC micromechanical model for predicting the large rate-independent thermoelastoplastic deformation of multiphase composites in which any one of the constituents is considered either as a rate-independent isotropic thermoelastoplastic material or a isotropic thermoelastic one. In order to carry out such an investigation, a suitable rate-independent finite strain thermoelastoplastic constitutive law must be established. Formulations of the theory of plasticity with large deformation have been presented by [Lubliner \[1990\]](#) where related references are given. A particular constitutive model for a rate-independent finite plasticity that avoids the difficulties posed by the rate formulation is given by [Simo \[1988b; 1988a\]](#) and summarized by [Simo and Hughes \[1998\]](#). It is based on the multiplicative decomposition of the deformation gradient and the stress-deformation relation is derived from a suitable energy function. This is followed by a radial-mapping algorithm for the integration of the flow rule and hardening law and the establishment of a consistent elastoplastic tangent tensor. This rate-independent finite strain plasticity formulation is adopted herein to model the rate-independent elastoplastic constituents of some of the multiphase composites whose behavior is micromechanically analyzed by the HFGMC model. A generalization is also proposed in order to include thermal effects by introducing a suitable free-energy function.

This paper is organized as follows. A very brief summary of the finite strain rate-independent plasticity is given in [Section 2](#). This is followed in [Section 3](#) by presenting the finite strain macroscopic constitutive rate equations that govern the multiphase thermoelastoplastic material which are established by employing the homogenization technique for periodic composites. In [Section 4](#), verifications of the HFGMC micromechanical predictions are made by a comparison with the concentric cylinder assemblage (CCA) model which is valid for an axisymmetric loading. To this end, the average radial stress of a porous thermoelastoplastic material that is subjected to axisymmetric thermomechanical loading (a one-dimensional problem in polar coordinates) is compared with the HFGMC prediction of a porous composite subjected to a biaxial and thermal loading (a two-dimensional problem). It should be noted that in the derivation of the thermoelastoplastic CCA model, the instantaneous tangent tensors are not utilized whereas they are an essential ingredient in the development of the HFGMC model, thus rendering the comparison between the two models significant since they are based on totally different approaches. [Section 5](#) presents several applications of the micromechanical model. To this end a hypothetical system of a rubber-like matrix reinforced by unidirectional metallic fibers is considered. The fibers are modeled

by the finite thermoplasticity theory which was discussed in [Section 2](#), whereas the matrix is modeled as a neo-Hookean hyperelastic material. Furthermore, the present finite strain elastoplastic micromechanics model is employed as a constitutive equation in a lamination theory to investigate the response of several types of symmetric laminates subjected to in-plane loading. Auxetic materials become thicker when stretched and thinner when compressed. This implies that the Poisson's ratio of this type of materials is negative. A recent review of auxetic materials and their utilization in various practical applications has been given by [Alderson and Alderson \[2007\]](#). This review includes the fabrication, characterization, testing, and possible applications of auxetic cellular solids, polymers, and fiber-reinforced materials. In the present section, a reentrant configuration of a metallic elastoplastic material undergoing finite deformation, which is capable to generate instantaneous negative Poisson's ratios, is considered. The conclusion offers several possible applications and generalizations of the present micromechanical approach.

2. Finite thermoplasticity of monolithic materials

Let \mathbf{X} and \mathbf{x} denote the location of a point in the material with respect to the initial (Lagrangian) and current systems of coordinates, respectively, and let t denote the time. In terms of the local deformation gradient tensor $\mathbf{F}(\mathbf{X}, t)$, $d\mathbf{x} = \mathbf{F}(\mathbf{X}, t)d\mathbf{X}$. The finite plasticity theory that was presented by [Simo \[1988b; 1988a\]](#) and summarized by [Simo and Hughes \[1998\]](#) is based on the introduction of a stress-free intermediate configuration and a multiplicative decomposition of the local deformation gradient $\mathbf{F}(\mathbf{X}, t)$ in the form $\mathbf{F}(\mathbf{X}, t) = \mathbf{F}^e(\mathbf{X}, t)\mathbf{F}^p(\mathbf{X}, t)$, where $\mathbf{F}^p(\mathbf{X}, t)$ and $\mathbf{F}^e(\mathbf{X}, t)$ are the deformation gradient tensors from the initial to the intermediate and from the intermediate to the current configuration, respectively. The corresponding right Cauchy–Green tensors are given by

$$\mathbf{C} = \mathbf{F}^T \mathbf{F}, \quad \mathbf{C}^p = \mathbf{F}^{pT} \mathbf{F}^p, \quad (1)$$

where superscript T denotes the transpose operation. The left Cauchy–Green tensors \mathbf{B} and \mathbf{B}^e are defined by

$$\mathbf{B} = \mathbf{F}\mathbf{F}^T, \quad \mathbf{B}^e = \mathbf{F}^e\mathbf{F}^{eT}$$

For an isotropic elastoplastic material, [Simo \[1988b; 1988a\]](#) and [Simo and Hughes \[1998\]](#) introduced an energy function which is decomposed into volumetric and deviatoric parts. Here a generalization is offered that provides a thermoelastoplastic free-energy function W in the form

$$W = \frac{\kappa}{2} \left[\frac{1}{2}(J^2 - 1) - \ln J \right] - 3\kappa\hat{\alpha}(\theta - \theta_0) \ln J + \frac{\mu}{2} [\text{tr}(\bar{\mathbf{B}}^e) - 3],$$

where κ , $\hat{\alpha}$, and $\theta - \theta_0$ are the bulk modulus, the thermal expansion coefficient, and the current temperature deviation from a reference temperature θ_0 , respectively, and $\bar{\mathbf{B}}^e = J^{-2/3}\mathbf{B}^e$, with $J = \det \mathbf{F}$.

The Kirchhoff stress tensor $\boldsymbol{\tau}$ can be derived from the energy function W to yield

$$\boldsymbol{\tau} = \left[\frac{1}{2}\kappa(J^2 - 1) - 3\kappa\hat{\alpha}(\theta - \theta_0) \right] \mathbf{I} + \mu \text{dev}(\bar{\mathbf{B}}^e), \quad (2)$$

where \mathbf{I} is the unit second-order tensor and $\text{dev}(\mathbf{T})$ denotes the deviatoric part of tensor \mathbf{T} .

For isotropic hardening, the von Mises yield criterion is given by $f(\boldsymbol{\tau}, \alpha) = \|\mathbf{s}\| - \sqrt{\frac{2}{3}}(Y + k(\alpha)) \leq 0$, where $\mathbf{s} = \text{dev}(\boldsymbol{\tau}) = \mu \text{dev}(\bar{\mathbf{B}}^e)$, and Y is the initial yield stress and $k(\alpha)$ is the isotropic hardening law with respect to the variable α . For a linear isotropic hardening $k(\alpha) = K\alpha$.

The associative flow rule was determined by [Simo \[1988a; 1988b\]](#) by the principle of maximum plastic dissipation [[Lubliner 1990](#)]. It is given by

$$\frac{\partial}{\partial t} \mathbf{C}^{p-1} = -\frac{2}{3} \gamma \operatorname{tr}(\mathbf{B}^e) \mathbf{F}^{-1} \frac{\mathbf{s}}{\|\mathbf{s}\|} \mathbf{F}^{-T},$$

and the evolution of the hardening variable α is determined, as in the infinitesimal theory of plasticity, from the consistency parameter γ in the form $\dot{\alpha} = \sqrt{\frac{2}{3}} \gamma$.

The radial return algorithm was extended by [Simo \[1988b; 1988a\]](#) and [Simo and Hughes \[1998\]](#) to the present theory of finite plasticity in order to obtain the variables τ_n , α_n and $\bar{\mathbf{B}}_n^e$ at any time step t_n at which the deformation gradient \mathbf{F}_n is given. One can readily determine \mathbf{C}_n^{p-1} from $\bar{\mathbf{B}}_n^e$ by employing the relation $\bar{\mathbf{B}}^e = J^{-2/3} \mathbf{F} \mathbf{C}^{p-1} \mathbf{F}^T$.

The formulation of the finite strain micromechanical analysis that is presented in the next section is based upon the rate of the actual stresses, referred to the undeformed configuration, which is expressed in terms of the rates of deformation gradient and temperature. Consequently, the constitutive equation of the monolithic thermoelastoplastic materials involves the first (unsymmetric) Piola–Kirchhoff stress tensor \mathbf{T} which is related to the Kirchhoff stress $\boldsymbol{\tau}$ as follows

$$\mathbf{T} = \mathbf{F}^{-1} \boldsymbol{\tau}. \quad (3)$$

The rate of the first Piola–Kirchhoff stress tensor $\dot{\mathbf{T}}$ is related to the rates of deformation tensor $\dot{\mathbf{F}}$ and temperature $\dot{\theta}$ in terms of the first tangent \mathbf{R} and thermal stress \mathbf{H} tensors, respectively, as follows

$$\dot{\mathbf{T}} = \mathbf{R} : \dot{\mathbf{F}} - \mathbf{H} \dot{\theta}, \quad (4)$$

where the expression $\mathbf{R} : \dot{\mathbf{F}}$ provides the double contraction of the fourth-order tensor \mathbf{R} with the second-order tensor $\dot{\mathbf{F}}$. The fourth-order tensor \mathbf{R} is given in terms of the consistent elastoplastic spatial tangent tensor \mathbf{c}^{ep} by

$$R_{ijkl} = F_{ip}^{-1} [c_{jpkq}^{ep} + \tau_{jk} \delta_{pq}] F_{lq}^{-1},$$

where δ_{pq} is the Kronecker delta. The consistent elastoplastic spatial tangent tensor \mathbf{c}^{ep} is given by [Simo and Hughes \[1998\]](#). The second-order thermal stress tensor \mathbf{H} is given by $\mathbf{H} = 3\kappa \hat{\alpha} \mathbf{F}^{-1}$.

In order to illustrate an application of these constitutive equations, we consider a metallic thermoelastoplastic linear hardening material whose properties are given in [Table 1](#) (in the range of small deformation, these parameters correspond to the characterization of the aluminum alloy 2024–T4 at room temperature). [Figure 1\(a\)](#) shows the uniaxial Kirchhoff stress variation against the deformation gradient of this material under one cycle of a mechanical loading and unloading. This figure shows also the material response when the plasticity effects are neglected, thus yielding a nonlinearly elastic behavior. Here, there is a slight nonlinearity which can be well observed. As a result, the linear hardening is slightly affected by this nonlinearly elastic behavior. [Figure 1\(b\)](#) shows the corresponding behavior of this material when

κ (GPa)	μ (GPa)	$\hat{\alpha}$ (K^{-1})	Y (MPa)	K (GPa)
71	27.2	22.5×10^{-6}	286.67	11.7

Table 1. Material parameters of the metallic material.

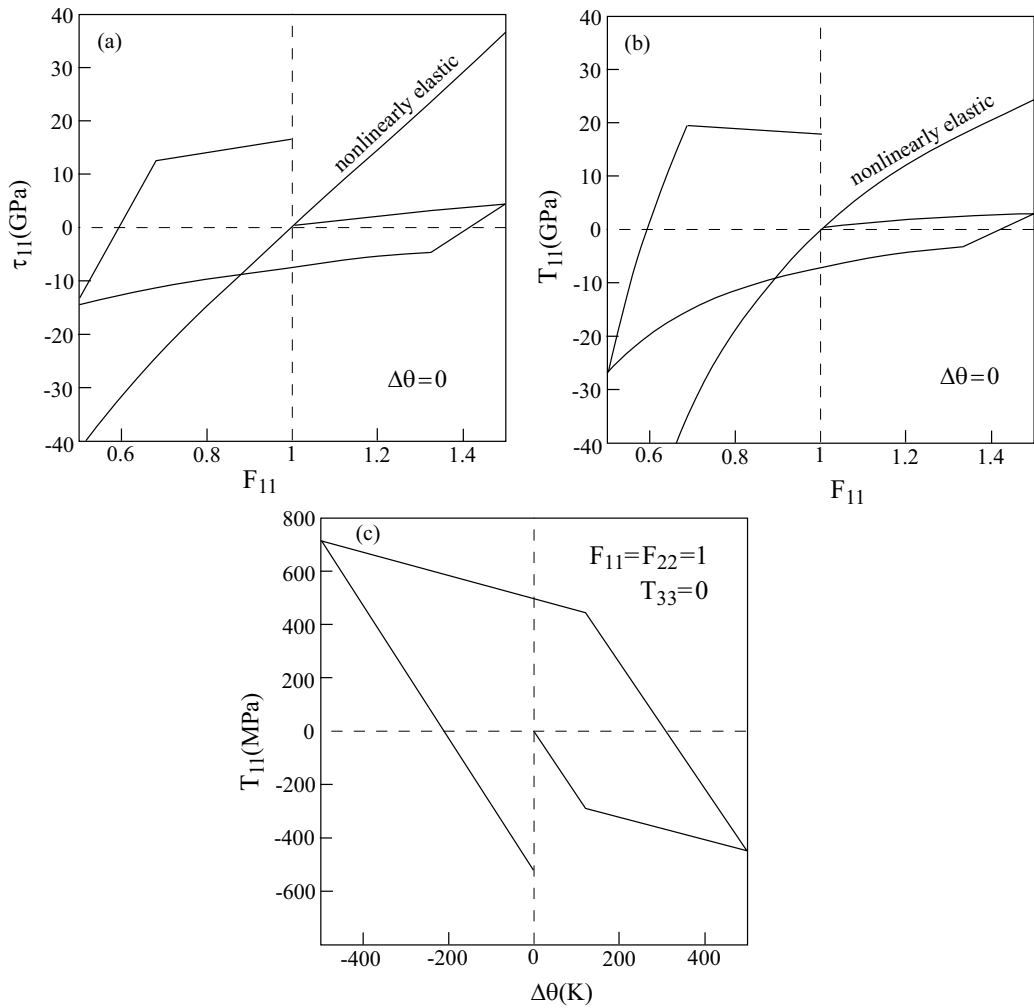


Figure 1. The behavior of the thermoelastoplastic monolithic metallic material, whose properties are given in Table 1. Shown are (a) the uniaxial Kirchhoff stress-deformation response, (b) the uniaxial first Piola–Kirchhoff stress-deformation response, and (c) the stress-temperature response.

it is represented in terms of the first Piola–Kirchhoff stress against the deformation gradient. It should be emphasized that the elastoplastic response shown in Figure 1(b) is based on a direct computation of T_{11} without utilizing the tangent tensor \mathbf{R} . This response however coincides with the corresponding one computed by utilizing \mathbf{R} . Also shown in Figure 1(b) is the behavior of the material when the plasticity effects are ignored. Here, the nonlinearity of the elastic material is well observed (the stress at a compression of $F_{11} = 0.5$ attains the value of -84 GPa). Figures 1(a) and 1(b) exhibit the material response under isothermal conditions $\Delta\theta = \theta - \theta_0 = 0$. Figure 1(c) shows the response of the material under one cycle of heating-cooling of a 500 K temperature deviation. Here, the material is subjected to the following conditions $F_{11} = F_{22} = 1$ and $T_{33} = 0$. It should be noted that the resulting maximum amount

of deformation gradient in this case is $F_{33} = 1.03$, that is, 3%, which can be still considered as a small deformation. Consequently the values of the first Piola–Kirchhoff and Kirchhoff stresses are practically identical.

3. Finite strain micromechanical modeling of fiber-reinforced materials

Finite strain micromechanical analyses of fiber-reinforced materials with periodic microstructure have been previously proposed [Aboudi 2002; 2003; 2004a; 2004b] for the determination of the behavior of thermoelastic, viscoplastic, and thermoviscoelastic multiphase composites, respectively. An extensive verification of the micromechanical analysis in the elastic case of continuous fiber composites was presented by Aboudi and Pindera [2004]. These micromechanical analyses are based on the homogenization technique in which a repeating unit cell of the periodic composite is identified.

In Figure 2, a multiphase composite with a doubly periodic microstructure defined with respect to the initial macroscopic (global) material coordinates of the X_2 - X_3 plane is shown together with its repeating unit cell, defined with respect to the initial microscopic (local) material coordinates Y_2 - Y_3 . In the framework of the homogenization method [Parton and Kudryavtsev 1993], the rate of the displacement vector is asymptotically expanded in terms of a small parameter δ . The size of the unit cell is further assumed to be much smaller than the size of the body so that the relation between the global and local systems is $\mathbf{Y} = \mathbf{X}/\delta$. This implies that a movement of order unity on the local scale corresponds to a very small movement on the global scale.

The homogeneization procedure ultimately provides the following strong form of the Lagrangian equilibrium equations

$$\nabla_{\mathbf{Y}} \cdot \dot{\mathbf{T}}^1 + \nabla_{\mathbf{Y}} \cdot \dot{\mathbf{T}}^0 = 0 \tag{5}$$

where $\dot{\mathbf{T}}^0 = \mathbf{R}(\mathbf{Y}, t) : \dot{\hat{\mathbf{F}}}(\mathbf{X}, t) - \mathbf{H}(\mathbf{Y}, t) \dot{\theta}(t)$, which is the rate of the stress tensor due to the externally applied rate of the deformation gradient $\dot{\hat{\mathbf{F}}}(\mathbf{X}, t)$ and temperature $\dot{\theta}(t)$, and $\dot{\mathbf{T}}^1 = \mathbf{R}(\mathbf{Y}, t) : \dot{\hat{\mathbf{F}}}(\mathbf{X}, \mathbf{Y}, t)$ is the resulting fluctuating stress tensor rate which is given in terms of the rate of the fluctuating displacement gradient $\dot{\hat{\mathbf{F}}}(\mathbf{X}, \mathbf{Y}, t)$. It is readily seen that the first terms in Equations (5) involve the unknown fluctuating

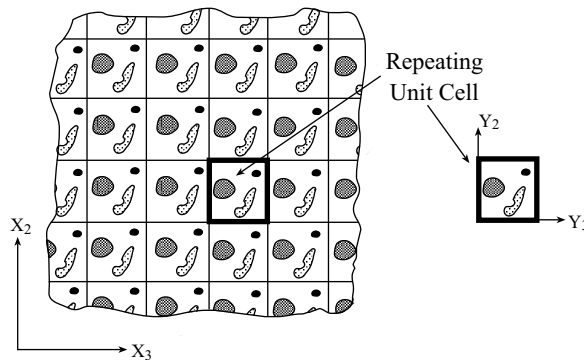


Figure 2. A multiphase composite with doubly-periodic microstructures defined with respect to global initial coordinates of the plane X_2 - X_3 . The repeating unit cell is defined with respect to local initial coordinates of the plane Y_2 - Y_3 .

periodic displacement rate $\dot{\mathbf{u}}$ while the second term in these equations produce pseudo-body forces whose derivatives are actually zero everywhere except at the interfaces between the phases.

For imposed values of the average deformation gradient rate $\dot{\mathbf{F}}$ and temperature rate $\dot{\theta}$, the unknown fluctuating displacement rate is governed by Equations (5) subject to periodic boundary conditions that are prescribed at the boundaries of the repeating unit cell. Referring to Figure 2, the periodic boundary conditions are expressed by the requirement that the displacements and tractions should be equal on opposite sides of the repeating unit cell. Thus at the top and bottom surfaces, right and left surfaces of the repeating unit cell, the displacement and traction rates should be identical. In addition to these periodic boundary conditions one needs to impose continuity of displacements and tractions at the internal interfaces between the phases that fill the repeating unit cell.

Once the solution of Equations (5), subject to the internal interfacial conditions and periodic boundary conditions, has been established, one can proceed and determine the instantaneous mechanical fourth-order and thermal second-order concentration tensors $\mathbf{A}^M(\mathbf{Y}, t)$ and $\mathbf{A}^{TH}(\mathbf{Y}, t)$ that relate the local rate of deformation gradient $\dot{\mathbf{F}}(\mathbf{Y}, t)$ at a material point \mathbf{Y} within the repeating unit cell at time t to the rate of the externally applied deformation gradient $\dot{\mathbf{F}}(t)$ and temperature $\dot{\theta}(t)$. Thus

$$\dot{\mathbf{F}}(\mathbf{Y}, t) = \mathbf{A}^M(\mathbf{Y}, t) : \dot{\mathbf{F}}(t) + \mathbf{A}^{TH}(\mathbf{Y}, t) \dot{\theta}(t).$$

It follows from Equation (4) that the local stress rate at this point is given by

$$\dot{\mathbf{T}}(\mathbf{Y}, t) = \mathbf{R}(\mathbf{Y}, t) : [\mathbf{A}^M(\mathbf{Y}, t) : \dot{\mathbf{F}}(t) + \mathbf{A}^{TH}(\mathbf{Y}, t) \dot{\theta}] - \mathbf{H}(\mathbf{Y}, t) \dot{\theta}(t).$$

Hence the resulting macroscopic constitutive rate equation for the multiphase thermoelastoplastic composite undergoing large deformation is given by

$$\dot{\mathbf{T}}(t) = \mathbf{R}^*(t) : \dot{\mathbf{F}}(t) - \mathbf{H}^*(t) \dot{\theta}(t), \quad (6)$$

where $\mathbf{R}^*(t)$ and $\mathbf{H}^*(t)$ are the instantaneous effective stiffness and thermal stress tensors of the multiphase composite which are given in terms of properties of the constituents in the form

$$\mathbf{R}^*(t) = \frac{1}{V_Y} \iint_{V_Y} \mathbf{R}(\mathbf{Y}, t) \cdot \mathbf{A}^M(\mathbf{Y}, t) dV_Y \quad (7)$$

and

$$\mathbf{H}^*(t) = -\frac{1}{V_Y} \iint_{V_Y} [\mathbf{R}(\mathbf{Y}, t) : \mathbf{A}^{TH}(\mathbf{Y}, t) - \mathbf{H}(\mathbf{Y}, t)] dV_Y, \quad (8)$$

where V_Y is the volume of the repeating unit cell.

In the framework of the HFGMC model, the repeating unit cell of Figure 2 is divided into several subcells, and the integrals in Equations (7) and (8) are discretized by summing over these subcells. More details can be found in the aforementioned references.

4. Verification of the micromechanical prediction

In the present section, verifications of the offered micromechanical analysis are given under isothermal and combined thermoelastic loadings.

4.1. Axisymmetric mechanical loading. The reliability of the micromechanically established finite strain macroscopic elastoplastic constitutive equations can be verified by considering a hollow cylinder under externally applied radial stretch and zero axial deformation.

The employed cylindrical geometry and loading correspond to the response of the concentric cylinder assemblage (CCA) model proposed by Hashin and Rosen [1964] which in the present context represents a porous composite with an axial pore content subjected to large axisymmetric deformations. In the framework of this model, the radial stress-radial stretch ($T_{RR} - \lambda_{RR}$) response of the outer surface of a single hollow cylinder subjected to axisymmetric loading coincides with that of the effective response ($\bar{T}_{RR} - \bar{\lambda}_{RR}$) of the entire porous composite subjected to the same type of loading. For a hollow core that accounts for a volume fraction v_f of the total cross-sectional area transverse to the reinforcement direction, one can perform a direct comparison with the present HFGMC micromechanical model predictions based on the repeating unit cell with a void volume fraction of v_f subjected to biaxial tension $\bar{F}_{22} = \bar{F}_{33}$ that provides $\bar{T}_{22} = \bar{T}_{33}$. A direct comparison between \bar{T}_{RR} and \bar{T}_{22} provides information about the accuracy of the micromechanical prediction.

It should be emphasized that the offered reliability verification is significant because although the concentric cylinder assemblage problem is one-dimensional, the present micromechanical doubly periodic model is two-dimensional. In addition, the micromechanical model constitutive equations are based on the effective instantaneous tangent tensors \mathbf{R}^* and \mathbf{H}^* ; see Equation (6). The derived CCA model given in the following, however, is not dependent on the use of instantaneous tangent tensors \mathbf{R} and \mathbf{H} of Equation (4), since it is based on the direct use of the stress tensor \mathbf{T} , see Equation (3), rather than its rate.

The specific discretization of the repeating unit cell that mimic the circular character of the central void surrounded by the nonlinear material is performed herein by employing 8×8 subcells. This discretization is shown herein to yield reliable results.

Consider the plane strain deformation of a hollow cylinder under a uniform radial stretch at the outer radius and zero traction at the inner radius. Let R , Θ , and Z denote the cylindrical coordinates of a material particle in the initial configuration, where $A \leq R \leq B$ and $0 \leq \Theta \leq 2\pi$ with A and B denoting the inner and outer radii, respectively. The current location of this particle is given by r , θ and z such that the deformation is described by $r(R, t)$, $\theta = \Theta$, and $z = Z$, where $a \leq r(R, t) \leq b$ and a and b denote the current inner and outer radii.

For this type of deformation, the deformation gradient is given in terms of the principal stretches $\lambda_{RR} = dr(R, t)/dR$, $r(R, t)/R$, and 1 by

$$\mathbf{F} = \text{diag}\left(\frac{dr(R, t)}{dR}, \frac{r(R, t)}{R}, 1\right). \quad (9)$$

In addition, \mathbf{C}^{p-1} in Equation (1) can be represented by

$$\mathbf{C}^{p-1} = \text{diag}(1 + G_{RR}(R, t), 1 + G_{\Theta\Theta}(R, t), 1 + G_{ZZ}(R, t)),$$

such that in the absence of plasticity effects $G_{RR} = G_{\Theta\Theta} = G_{ZZ} = 0$. These functions can be determined at any loading increment by employing the definition of $\bar{\mathbf{B}}^e$. In conjunction with Equation (9), the tensor

$\bar{\mathbf{B}}^e$ can be readily determined in the form

$$\bar{\mathbf{B}}^e = \text{diag}\left(\frac{r'(1 + G_{RR})}{J^{2/3}}, \frac{r^2(1 + G_{\Theta\Theta})}{R^2 J^{2/3}}, \frac{(1 + G_{ZZ})}{J^{2/3}}\right), \quad (10)$$

where $J(R, t) = r'r/R$ and $r' = dr(R, t)/dR$.

The deviatoric stress \mathbf{s} can be readily determined from Equation (10) and, consequently, the Kirchhoff stress $\boldsymbol{\tau}$ follows from Equation (2)

$$\tau_{RR} = \frac{\kappa}{2}[J^2 - 1] + \frac{\mu}{J^{2/3}}\left[a(r')^2(1 + G_{RR}) + b\frac{r^2(1 + G_{\Theta\Theta})}{R^2} + c(1 + G_{ZZ})\right], \quad (11)$$

where $a = 2/3$, $b = c = -1/3$. The component $\tau_{\Theta\Theta}$ is given by same expression but with $a = c = -1/3$, $b = 2/3$. Similarly, τ_{ZZ} is of the same form shown by Equation (11) with $a = b = -1/3$, $c = 2/3$. The Kirchhoff stress tensor $\boldsymbol{\tau}$ provides the first Piola–Kirchhoff stress tensor \mathbf{T} by employing Equation (3).

The equilibrium equations reduce to the single equation

$$\frac{dT_{RR}}{dR} + \frac{T_{RR} - T_{\Theta\Theta}}{R} = 0, \quad (12)$$

where T_{RR} and $T_{\Theta\Theta}$ are the components of the first Piola–Kirchhoff stress tensor. The explicit form of the resulting second-order nonlinear ordinary differential equation that is obtained from Equation (12) is very lengthy and thus it is not given here. It can be formally represented as follows

$$\Phi(r'', r', r, G'_{RR}, G'_{\Theta\Theta}, G'_{ZZ}, G_{RR}, G_{\Theta\Theta}, G_{ZZ}) = 0, \quad (13)$$

where the primes denote differentiation with respect to R .

The solution of this equation for $r(R)$ is obtained subject to a traction-free condition at the inner radius, and a specified deformation at the outer radius in the current configuration, that is,

$$T_{RR} = 0, \quad R = A \quad (14)$$

and

$$r(B, t) = b = \bar{\lambda}_{RR}B, \quad R = B, \quad (15)$$

where $\bar{\lambda}_{RR}$ is the current prescribed radial stretch. Consequently, the second-order nonlinear ordinary differential Equation (13) and the boundary conditions, Equations (14) and (15), form a two-point boundary value problem. Its solution determines at any stage of loading the current location $r(R)$ of any point $A \leq R \leq B$, which leads to the determination of the stress field, including the radial stress T_{RR} at the outer surface $R = B$. The use of the average stress theorem produces the average radial stress \bar{T}_{RR} for the entire hollow cylinder, namely, $\bar{T}_{RR} = T_{RR}(R = B)$. Consequently, the effective stress-deformation relationship of the porous material, with the initial volume concentration of pores given by $A^2/B^2 < 1$, subjected to the specified plane strain axisymmetric loading by $\bar{\lambda}_{RR} = b/B$, is established. The solution of the present second-order nonlinear ordinary differential equation can be obtained by a finite-difference procedure for two-point boundary value problems [Roberts and Shipman 1972]. According to this method, the interval $A \leq R \leq B$ is divided into several subintervals and the derivatives with respect to R are replaced by their corresponding finite differences in these intervals. As a result, a system of nonlinear algebraic equations is obtained, which is solved at any loading increment by an iterative procedure until convergence is achieved up to a preassigned degree of accuracy.

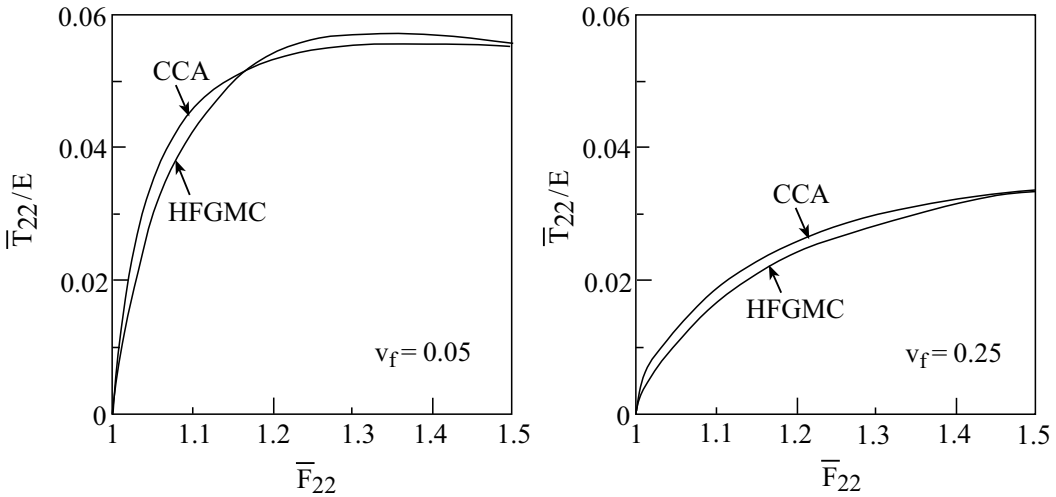


Figure 3. Macroscopic response of a porous material with (a) 5% and (b) 25% porosities subjected to a biaxial loading. The figure compares the HFGMC and the CCA model predictions. The stresses are normalized with respect to the Young's modulus E of the metallic material, whose properties are given in [Table 1](#).

[Figure 3](#) presents a comparison between the isothermal response predictions of the HFGMC and CCA models for void volume fraction of $v_f = 0.05$ and 0.25 . The metallic elastoplastic material is characterized by [Table 1](#). It can be observed that quite good correspondence between the two models exists in both cases. In the case of a void volume fraction of $v_f = 0.25$ the slight difference between the yield stresses predicted by the two methods may be attributed to the fact that in the CCA and HFGMC models, the governing equations and boundary conditions are imposed in a pointwise manner and in average sense, respectively.

It is worth mentioning that by taking $\mu = 0$ in [Equation \(11\)](#), a hyperelastic material whose strain-energy function depends on J , so that it is of the Varga type [[Horgan 1995](#); [Horgan 2001](#)], is obtained. This class of materials admits, under the present axisymmetry conditions, an exact solution of the equilibrium [Equation \(12\)](#) of the form $r(R) = \sqrt{\xi R^2 + \eta}$, where ξ and η are arbitrary constants. It follows from [Equation \(9\)](#) that $J = \xi$. This implies, according to [Equation \(11\)](#) and boundary condition [\(14\)](#) that in this case the CCA model yields zero stresses everywhere in the region. This situation is also obtained from the HFGMC model in this type of porous material.

4.2. Axisymmetric thermomechanical loading. As a check of the reliability of the micromechanical prediction of a composite under thermoelastic loading, we consider again the CCA model in which a thermal loading θ is applied this time at the region $A \leq R \leq B$ in addition to the mechanical loading applied at the outer surface $R = B$ (given by the boundary conditions [\(15\)](#)). The resulting nonlinear ordinary differential equation that governs the two-point boundary value problem is solved as before by a finite difference method. The resulting radial stress T_{RR} at the outer surface $R = B$ is the average stress \bar{T}_{RR} of the composite cylinder and it can be compared with the macroscopic stress $\bar{T}_{22} = \bar{T}_{33}$ of the HFGMC model in which the same thermal loading is applied.

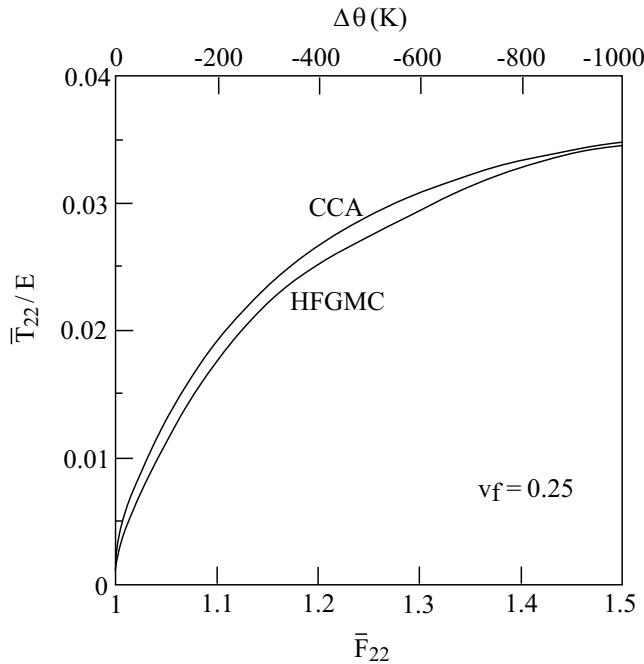


Figure 4. Macroscopic response of a porous metallic material with a 25% porosity subjected to a combined biaxial and thermal loading. The figure compares the HFGMC and the CCA model predictions. The stress is normalized with respect to the Young's modulus E of the metallic material whose properties are given in Table 1.

In Figure 4, a comparison between the CCA and HFGMC prediction is shown for the thermoelastic metallic material that is specified in Table 1. It shows the normalized transverse stress (with respect to the Young's modulus E of the material) caused by a combined thermomechanical loading in which the porous material is biaxially stretched up to $\bar{F}_{22} = \bar{F}_{33} = 1.5$ with $\bar{F}_{11} = 1$ together with a simultaneous temperature deviation of $\theta - \theta_0$. In the absence of a mechanical loading, the normalized stress at the final temperature loading is $\bar{T}_{22}/E = \bar{T}_{33}/E = 0.0083$, which can be readily obtained from the metallic material clamped in the 1-direction. The combined thermomechanical loading generates the value of $\bar{T}_{22}/E = \bar{T}_{33}/E = 0.035$ at the final stretch and temperature. Thus the thermal loading generates a response of about 23% of the combined thermomechanical loading which is an appreciable value. The graphs in Figure 4 clearly show the yield points and the saturation caused by the plasticity effects. The correspondence between the two models, which are based on two different systems of constitutive equations, is reasonable.

5. Applications: isothermal behavior of a metal/rubber-like composite

The established finite strain macroscopic constitutive equations for thermoelastoplastic multiphase materials are implemented to investigate the behavior of a rubber-like matrix reinforced by metallic material whose properties are given in Table 1 (page 812). The behavior of the composite is presented under isothermal conditions.

In the present isothermal case, the hyperelastic matrix is modeled by the compressible neo-Hookean material the constitutive equations of which have been presented by [Peric \[1992\]](#) and [van der Sluis et al. \[2001\]](#). With \mathbf{F} , \mathbf{C} , and J representing, as before, the deformation gradient, the right Cauchy–Green deformation tensor, and the determinant of \mathbf{F} , respectively, let I_1 denote the first invariant, that is, the trace of \mathbf{C} . Accordingly, the strain-energy W of this material is given by

$$W = \frac{\mu}{2}(I_1 - 3 - 2 \ln J) + \frac{\lambda}{2}(\ln J)^2, \tag{16}$$

where λ and μ are the Lamé’ constants.

The second Piola–Kirchhoff stress tensor \mathbf{S} is determined from $\mathbf{S} = 2 \frac{\partial W}{\partial \mathbf{C}}$. By utilizing the relation between the first and second Piola–Kirchhoff stress tensor, $\mathbf{T} = \mathbf{S}\mathbf{F}^T$, the following constitutive equation that relates the rate of the first Piola–Kirchhoff stress tensor $\dot{\mathbf{T}}$ to the rate of the deformation gradient $\dot{\mathbf{F}}$ is obtained

$$\dot{\mathbf{T}} = \mathbf{R} : \dot{\mathbf{F}}, \tag{17}$$

where \mathbf{R} is the current fourth-order tangent tensor given by $R_{ijkl} = D_{irts} F_{jr} F_{ks} + S_{il} \delta_{jk}$ with the material fourth-order tangent tensor \mathbf{D} defined by

$$\mathbf{D} = 2 \frac{\partial \mathbf{S}}{\partial \mathbf{C}} = 4 \frac{\partial^2 W}{\partial \mathbf{C} \partial \mathbf{C}}.$$

As in [van der Sluis et al. \[2001\]](#), the Lamé’ constants in [Equation \(16\)](#) are chosen as $\lambda = 980$ MPa and $\mu = 30$ MPa. [Figure 5](#) shows the behavior of this material under a uniaxial stress loading in the 1-direction. The effect of nonlinearity and compressibility can be well observed.

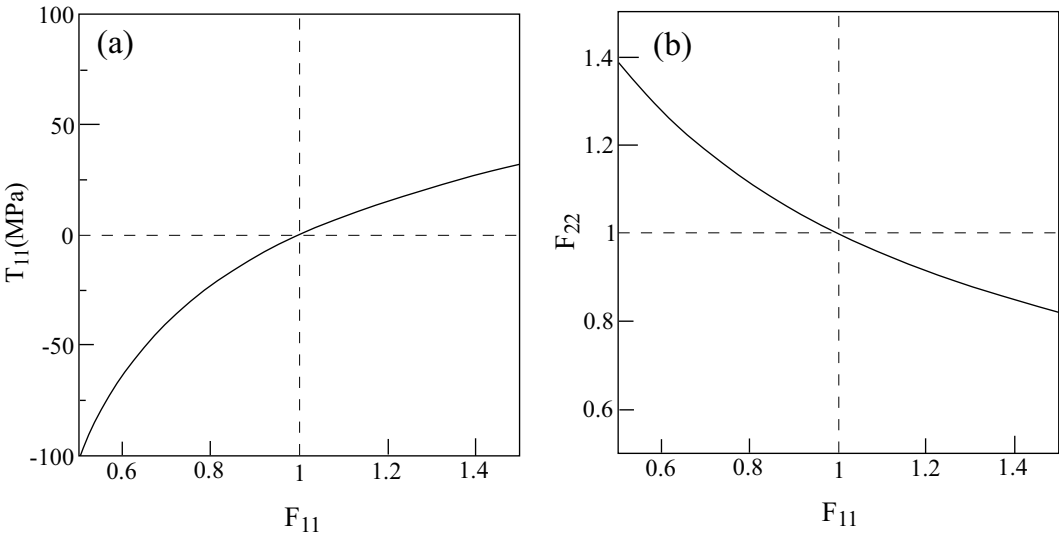


Figure 5. The uniaxial stress response of the rubber-like material modeled by the neo-Hookean constitutive law [Equation \(16\)](#). Shown are (a) the uniaxial stress against axial deformation gradient and (b) the transverse against axial deformation gradient.

5.1. Unidirectional metal/rubber-like composite. Consider a hypothetical composite system that consists of a rubber-like matrix reinforced by unidirectional continuous metallic fibers that are oriented in the 1-direction. The constitutive equations of the hyperelastic rubber-like material and the elastoplastic metallic fibers are given by Equations (17) and (4), respectively. In all cases, the volume fraction of the fibers is $v_f = 0.1$. As discussed previously, the specific discretization of the repeating unit cell that mimic a circular fiber surrounded by matrix material is performed by employing 8×8 subcells. This discretization was verified to provide a accurate results.

Let the composite be subjected to an off-axis uniaxial stress loading. Here, the unidirectional composite, in which the fibers are oriented in the 1-direction, is rotated around the 3-direction by an angle ϕ . As a result, a new system of coordinates (X, Y, Z) is obtained such that $Z = X_3$. The uniaxial stress loading is applied in the X -direction which is at angle ϕ with respect to the fibers direction. Referring to this new system of coordinates, the composite is loaded by the application of the deformation gradient F_{XX} , and all other components of the stress tensor \mathbf{T}^X , referred to the new coordinate system, are equal to zero except T_{XX} . In particular, $\phi = 0^\circ$ and 90° correspond to longitudinal and transverse uniaxial stress loading.

Figure 6 shows the response of the composite including the associated Poisson’s effect to off-axis uniaxial stress loading for $\phi = 0^\circ, 10^\circ, 30^\circ$ and 45° . The effect of plastic flow of the metallic fibers can be well detected by observing the yield stresses in the cases of $\phi = 0^\circ$ and 10° . For the off-axis loading at $\phi = 30^\circ$, the location of the yield stress is shown by the arrow. For the off-axis angle $\phi = 45^\circ$, however, plasticity does not occur and the response of the composite in this case is merely nonlinearly elastic. It is interesting that while the stress T_{XX} decreases monotonically with the increase of the off-axis angle ϕ , the transverse deformation F_{YY} exhibits a peculiar behavior in the sense that there is a sudden jump in the

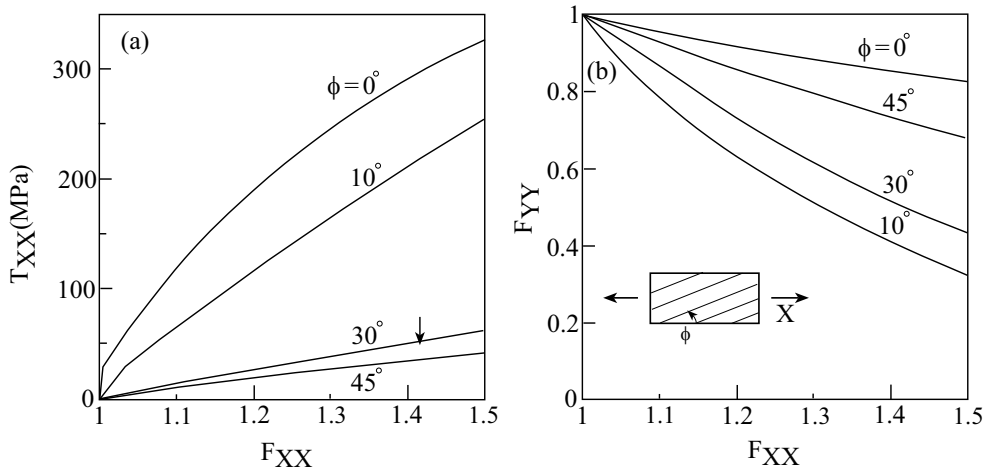


Figure 6. Off-axis uniaxial stress response of a unidirectional metal/rubber-like composite. The rotation ϕ around the 3-direction denotes the angle between the fibers (oriented in the 1-direction) and the loading (applied in the X -direction). The arrow indicates the yield stress in the case of $\phi = 30^\circ$. Shown are (a) the stress against the applied deformation gradient and (b) the transverse deformation gradient against the applied one.

magnitude of this deformation from $\phi = 0^\circ$ to $\phi = 10^\circ$; see Figure 6(b). This feature was checked by generating the response at off-axis angle increments of 0.1° . It turned out that a transition from the off-axis angle $\phi = 4.1^\circ$ to $\phi = 4.2^\circ$ gives rise to a jump of F_{YY} from 0.82 to 0.7. A comparison with the corresponding finite strain elastic case in which the plasticity effects of the aluminum are ignored revealed that this jump occurs at the transition from $\phi = 4.1^\circ$ to $\phi = 4.2^\circ$, where the transverse deformation F_{YY} abruptly changes from 0.82 to 0.3. This jump may be attributed to the variation of the combined stresses (which induce the plastic flow) to which the elastoplastic phase is exposed as the off-axis angle changes. Thus the plastic flow of the aluminum has a significant effect on the instantaneous Poisson's ratio of the composite.

It is interesting to compare the resulting responses of the composite in the two extreme cases in which the uniaxial stress loading is applied in the fiber direction: $\phi = 0^\circ$, where the response is dominated by the fibers, and the perpendicular direction $\phi = 90^\circ$, where the response is dominated by the matrix, while ignoring any plasticity effects by simply assuming that the yield stress of the metallic fiber is very high. The composite behavior in these two extreme cases is shown in Figure 7 together with the corresponding axial and transverse Poisson's effects. By comparing the curves shown in Figure 6 with those shown in Figure 7, the effect of the plastic flow in the fibers can be realized. Thus for a longitudinal loading in the fiber direction, the plasticity effects decrease the stress at a stretch of $\bar{F}_{11} = 1.5$ from $\bar{T}_{11} = 2465$ MPa to 325 MPa, but for a loading in the transverse direction, no yielding occurs.

5.2. Laminated metal/rubber-like composite subjected to in-plane loading. We now embed the finite strain elastoplastic micromechanical model just developed in a standard lamination theory for a symmetrically layered medium that is subjected to in-plane loading. In this case, each layer undergoes

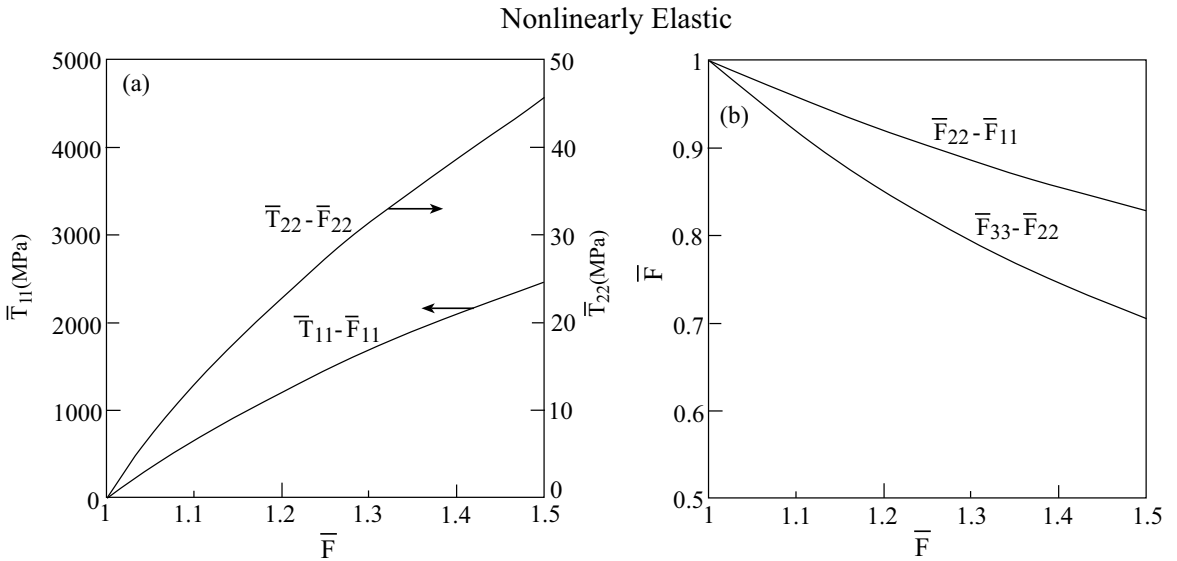


Figure 7. Axial and transverse response of the unidirectional metal/rubber-like composite in which the plasticity effects in the metallic fibers are neglected. Shown are (a) the axial stress against the applied axial deformation gradient, and transverse stress against the applied transverse deformation gradient and (b) the transverse deformation gradient against the corresponding applied ones.

the same deformation, rendering the finite strain elastoplastic lamination theory solution exact (since all equilibrium equations in the layers and continuity conditions between the layers are satisfied). The laminated material is referred to the global coordinates $\mathbf{X} = (X, Y, Z)$ such that the fiber direction in a layer is oriented at angle ϕ with respect to the lamination axis X in the direction of which the axial deformation gradient F_{XX} is applied, and Y is the other in-plane axis perpendicular to X . The laminated medium consists of L layers, each of which has an initial thickness t_k , $k = 1, 2, \dots, L$, forming a total initial thickness H . The initial positions of the layers with respect to the global system (X, Y, Z) are denoted by h_k .

Let $\mathbf{F}^{\mathbf{X}}$ denote the deformation gradient of the laminate described with respect to the global coordinates (X, Y, Z) and $\bar{\mathbf{F}}^{(k)}$ denote the deformation gradient of the layer k , referred to the material coordinates (X_1, X_2, X_3) of this layer with X_1 oriented in the fiber direction. At any instant of loading, the components of $\mathbf{F}^{\mathbf{X}}$ are known from the prescribed loading F_{XX} and from the conditions that the laminate is traction-free. Hence the deformation gradient tensor $\bar{\mathbf{F}}^{(k)}$ of any layer can be determined from $\mathbf{F}^{\mathbf{X}}$ by using the standard transformation law of second order tensors

$$\bar{\mathbf{F}}^{(k)} = \mathbf{A}_k^T \mathbf{F}^{\mathbf{X}} \mathbf{A}_k, \quad (18)$$

where \mathbf{A}_k is the transformation matrix from the global system to the material coordinates of the k -th layer.

Let $\bar{\mathbf{T}}^{(k)}$ denote the first Piola–Kirchhoff stress tensor in the k -th layer defined with respect to the material coordinates. With the known deformation gradient $\bar{\mathbf{F}}^{(k)}$ of the k -th layer given by Equation (18), the micromechanical analysis of the unidirectional lamina is employed subject to the condition that each layer is under plane stress. The finite strain elastoplastic micromechanical analysis readily provides $\bar{\mathbf{T}}^{(k)}$, which can be transformed back to the global coordinates by employing the transformation law of second-order tensors as follows $\mathbf{T}^{\mathbf{X}(k)} = \mathbf{A}_k \bar{\mathbf{T}}^{(k)} \mathbf{A}_k^T$, where $\mathbf{T}^{\mathbf{X}(k)}$ is the first Piola–Kirchhoff stress tensor in the k -th layer referred to the laminate coordinates. This procedure is repeated for all layers $k = 1, 2, \dots, L$. The resultant force (per unit length) vector \mathbf{N} for the current applied deformation gradient is obtained from $\mathbf{N} = \sum_{k=1}^L (h_k - h_{k-1}) \mathbf{T}^{\mathbf{X}(k)}$.

The average axial stress N_{XX}/H against the applied deformation gradient F_{XX} is shown in Figure 8 for a symmetric angle-ply laminate $[\pm\phi]_s$ whose layers consist of the unidirectional metal/rubber-like composite. Also shown is the transverse deformation against the axial one that provides the Poisson's effect of the laminate at any stage of loading. For $\phi = 0^\circ$ and 30° , the yield stresses can be well observed. For $\phi = 45^\circ$, the yield stress occurs at $N_{XX}/H = 24.1$ MPa. For $\phi = 60^\circ$, on the other hand, plasticity does not take place and the behavior of the angle-ply laminate is nonlinearly elastic. The nonlinearity of the response is clearly exhibited in all cases. It should be noted that for $\phi = 30^\circ$, a slope change occurs at about $F_{XX} = 1.17$ due to plasticity effects (It is of course absent in the corresponding finite strain elastic case. Here, $N_{XX}/H = 1136$ MPa at $F_{XX} = 1.5$, while, as shown in Figure 8(a), N_{XX}/H reaches 275 MPa at this point). Figure 8(b) exhibits the Poisson's effects of the considered elastoplastic laminates. Here too there is a discontinuous behavior in the response between $\phi = 0^\circ$ and $\phi = 10^\circ$. Similar behavior exists also when the plasticity flow of the aluminum is neglected while retaining the large deformation effects.

In order to enhance the plasticity effects of the laminate material, a ply in which the fibers are oriented in the X -direction is added to previous type of angle-ply laminate. As a result a symmetric laminated

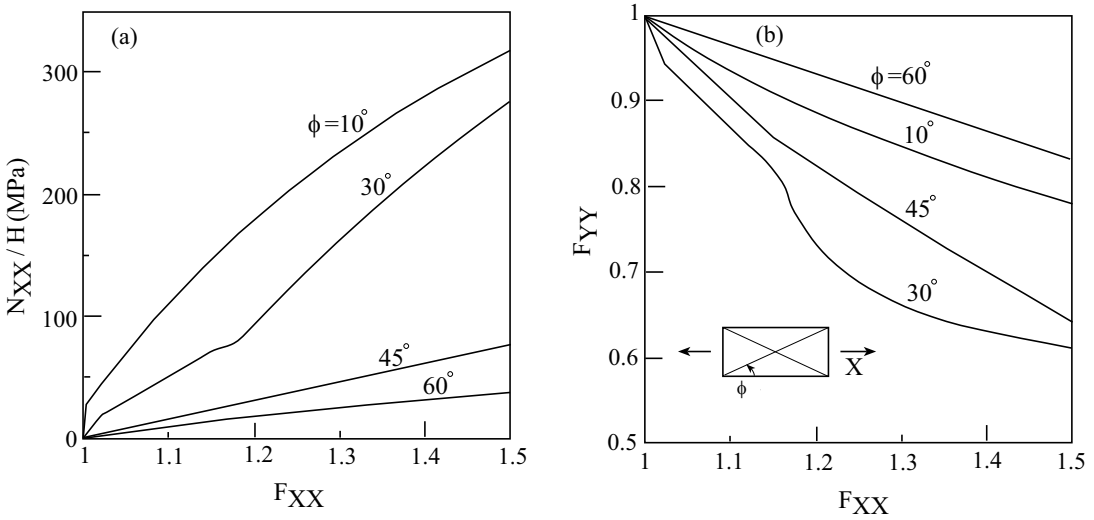


Figure 8. Shown are (a) the average axial stress and (b) the transverse deformation gradient against the applied deformation gradient of several symmetric angle-ply $[\pm\phi]_s$ laminates.

material of the type $[\pm\phi, 0]_s$ is obtained whose response is depicted in Figure 9 for various values of the angle ϕ . Here, plasticity effects occur in all angles ϕ with the corresponding yield stresses close to each other. In the special case of $\phi = 90^\circ$, a cross-ply laminate is obtained in which plastic flow starts at a stress level of about $N_{XX}/H = 10.4$ MPa which is very close to the other yield stresses.

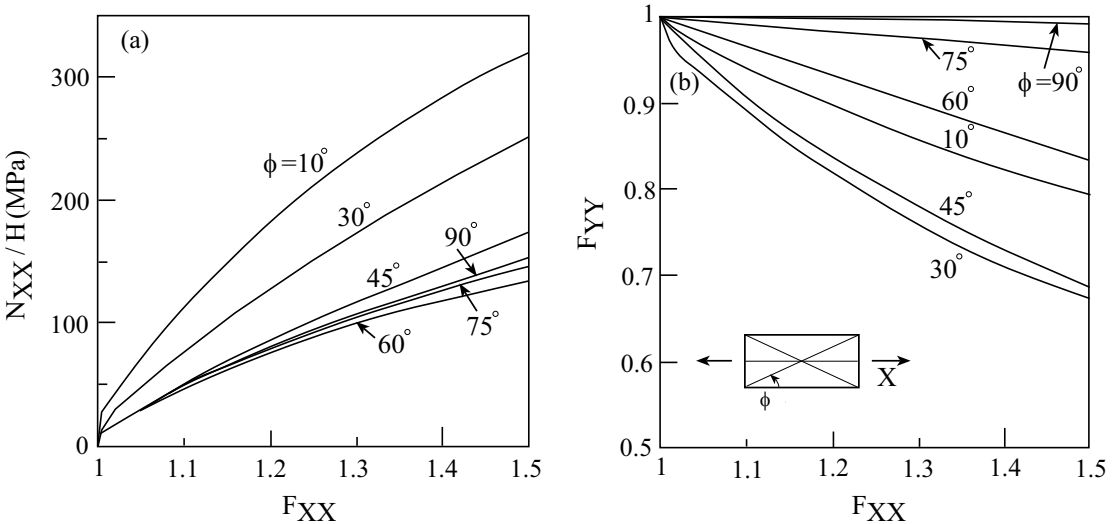


Figure 9. Shown are (a) the average axial stress and, (b) transverse deformation gradient against the applied deformation gradient of several symmetric $[\pm\phi, 0]_s$ laminates. For $\phi = 90^\circ$, a symmetric cross-ply $[90, 0]_s$ laminate is obtained.

5.3. Auxetic metallic material. Auxetic materials are a new class of materials which have a negative Poisson’s ratio. This implies that they expand in the lateral direction when stretched longitudinally. A reentrant configuration provides a means to construct such materials. To this end, the metallic elastoplastic material whose properties are given in Table 1 is employed in a reentrant configuration to study its finite strain elastoplastic response.

A specific configuration is employed in which the volume fraction of the metallic material is $1 - v_f = 0.28$. The inset in Figure 10(a) shows this configuration in which the angle between X_2 (along which the loading is applied) and the inclined arm is 15° and the ratio between the thickness to length of the solid strip is $1/6$. It should be noted that in the framework of the present micromechanical analysis, the entire X_2 - X_3 plane is assumed to be filled by this configuration in the periodic manner shown by

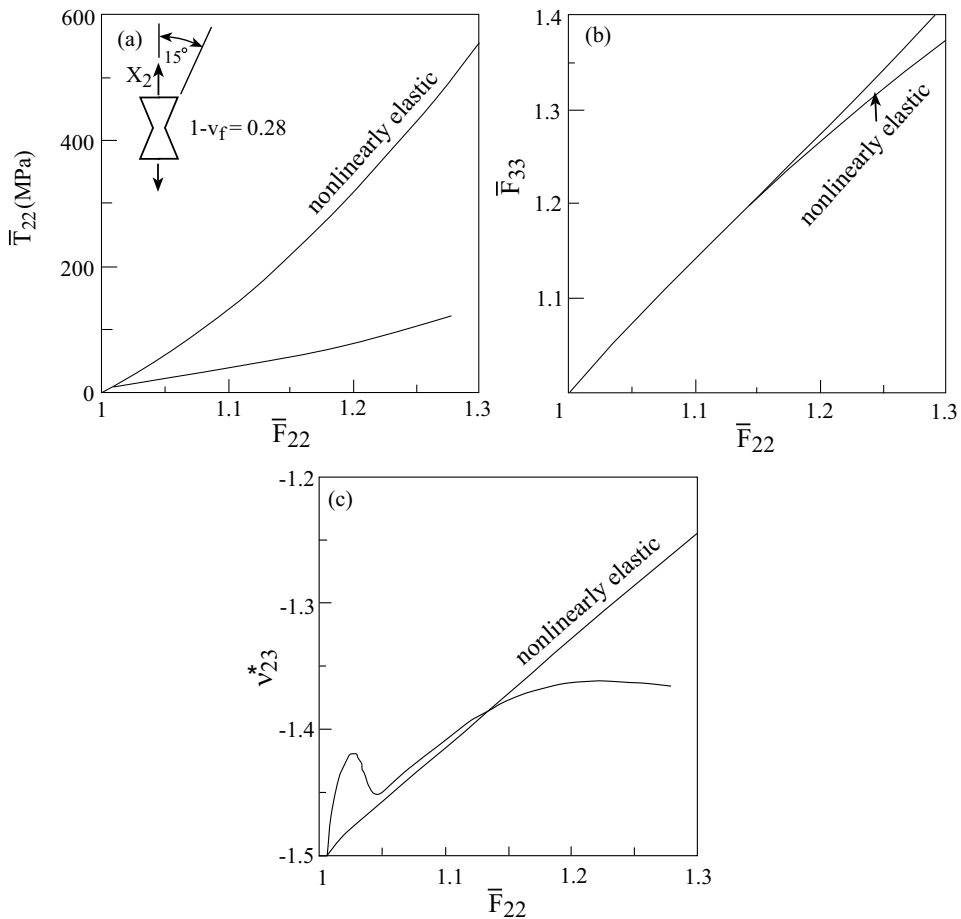


Figure 10. The behavior of a reentrant configuration that forms a type of auxetic material. The volume fraction of the metallic material is $1 - v_f = 0.28$. Shown are (a) the average stress in the 2-direction against the applied stretch in this direction, (b) the transverse in-plane stretch against the applied one, and (c) the effective transverse Poisson’s ratio against the applied stretch.

Figure 2. **Figure 10(a)** shows the macroscopic stress-deformation gradient response $\bar{T}_{22} - \bar{F}_{22}$ of this configuration. The special case in which the plasticity effects in the metallic material are ignored is shown for comparison. It is clearly seen that these effects are significant. **Figure 10(b)** shows the macroscopic transverse stretch in the 3-direction against the applied stretch in the 2-direction. The in-plane effective transverse Poisson's ratio ν_{23}^* can be determined at any instant of loading from

$$\nu_{23}^* = -\frac{\bar{F}_{33} - 1}{\bar{F}_{22} - 1}.$$

This ratio is shown in **Figure 10(c)**. It starts at $\nu_{23}^* = -1.5$ which correspond to the Poisson's ratio of the considered configuration at the region of infinitesimal elastic deformations. Plastic flow starts at a stretch of $\bar{F}_{22} = 1.008$ and a corresponding stress $\bar{T}_{22} = 8.4$ MPa (yield stress). When plasticity effects are ignored, the resulting effective Poisson's ratio rises linearly up to about -1.25 . In the actual situation when plasticity effects are present, the Poisson's ratio exhibits a peculiar behavior in the form of an increase followed by a decrease. For stretches \bar{F}_{22} larger than 1.15, ν_{23}^* is seen to be more negative than the corresponding one where the plasticity effects are ignored. Thus in the present circumstances, the elastoplastic material provides a more effective auxetic metallic material at large strains than the corresponding nonlinearly elastic one. In conclusion, the present finite strain elastoplastic micromechanics forms a quantitative tool for the prediction of the instantaneous negative Poisson's ratios of auxetic metallic material.

6. Conclusions

A finite strain micromechanical model is offered for the prediction of the macroscopic response of multiphase composites in which any constituent is considered as a rate-independent thermoelastoplastic material, a thermoelastic material, or a hyperelastic material. The response is governed by the established global constitutive equations of the composite in conjunction with the derived instantaneous mechanical and thermal tangent tensors. The macroscopic constitutive equations are subsequently employed in a finite strain lamination theory to investigate the behavior of symmetric elastoplastic laminates subjected to in-plane loading. The variation of the negative Poisson's ratio of an auxetic configuration undergoing large elastoplastic deformation is shown. The reliability of the micromechanical model prediction is examined by employing the CCA model which is valid under an axisymmetrical thermomechanical loading. The results for unidirectional and laminated elastoplastic composite as well as for auxetic materials show that the effect of the plastic flow is significant. In some situations, peculiar behavior caused by the finite strain plasticity effects is exhibited when the applied strains attain appreciable values. This behavior is absent when the plastic flow of the metallic constituent is neglected.

The present article continues a series of investigations [Aboudi 2002; 2003; 2004a] concerning the development of the finite strain micromechanical analysis (HFGMC) that is capable of predicting the behavior of multiphase materials undergoing large deformations. Any constituent in the composite can be selected to behave as a thermoelastic, thermoviscoelastic, and thermoinelastic material. In the latter case either rate-dependence (viscoplasticity) or rate-independence (plasticity which is the subject of the present paper) can be assumed. It is worth mentioning that the strategy of the finite strain modeling of composites with rate-dependent (viscoplastic and viscoelastic) constituents that was previously followed

[Aboudi 2003; 2004a], differs from the the one adopted in the present investigation of the behavior of composites that consist of rate-independent elastoplastic phases. In the former strategy, the inelastic effects were totally separated from the tangent tensor of the viscoplastic and viscoelastic constituents. In the present investigation, on the other hand, the rate-independent plasticity effects are incorporated with the tangent tensor (see Equation (4)), which is given in terms of the consistent elastoplastic spatial tangent tensor of Simo and Hughes [1998]. It is possible, however, to adopt just a single strategy and develop a unified finite strain HFGMC model for all these types of composites.

It is worth mentioning that in both the finite strain HFGMC model for viscoplastic phases [Aboudi 2003] and the present one for time-independent elastoplastic constituents, no special invariant rate of stresses (like the Jaumann rate) need to be introduced. This follows from the fact that the flow rules in both cases are formulated in the strain space.

The advantage of HFGMC model stems in its capability of modeling a periodic composite material by discretizing the repeating unit cell into quite few subcells. For example, in the present investigation 8×8 subcells were found to be sufficient to in providing good accuracy. This also implies that the running time of the program is quite short (several minutes). In addition, due to the rectangular shape of the subcells, the repeating unit cell discretization is quite simple. Due to the simplicity of HFGMC model, it should not be difficult to link it to a finite element procedure in order to analyze a composite structure (for example, composite beams, plates, and shells). Indeed, the capability for such structural investigations has been already performed in the infinitesimal strain domain by the Life Prediction Branch of NASA Glenn Research Center, who integrated HFGMC and its predecessor GMC model into a commercial finite element package. This software is referred to as *Finite Element Analysis Micromechanics Analysis Code* (FEAMAC) (see: www.lerc.nasa.gov/WWW/LPB/mac). Extensions of such a capability to the the finite strain domain should be also possible.

The present theory can be further extended for the investigation of the behavior of rubber matrix elastoplastic unidirectional and laminated composites with emphasis on the thermal effects. In such an investigation, a proper entropic elasticity modeling of the rubber-like matrix must be employed in order to simulate the Gough–Joule effect in such materials. Such an energy function, which was employed in [Aboudi 2002; 2004a] to analyze the behavior of thermoelastic and thermoviscoelastic of rubber-like matrix composites, can be utilized to model the finite strain thermoelastoplastic behavior of rubber-like matrix with embedded elastoplastic constituents.

A related issue is the potential application of the present methodology in the study of the behavior of certain biological tissues. Indeed, the finite strain HFGMC model with quasilinear viscoelastic (QLV) constituents has been recently employed by Surucu et al. [2005] for the investigation of the behavior of mitral valve chordae. Thus, it should be possible to implement the present micromechanical model to investigate the behavior of elastoplastic biological tissues. Concerning the study of the behavior of auxetic materials, other types of auxetic cellular solids (for example, metallic honeycombs and foams) can be analyzed by the present approach. Furthermore, auxetic composite laminates and composite containing metallic auxetic phases can be considered by employing the present micromechanical model. In addition, it is known that laminated elastic materials with certain stacking sequences can produce negative Poisson's ratios [Herakovich 1998]. It should be interesting to examine the effect of large plastic deformations on such laminated materials when plasticity effects are present. By employing the finite strain HFGMC model with nonlinearly elastic constituents, Bruck et al. [2007] presented an optimal design approach of

porous microstructures for porous materials. The material that was considered in this investigation was hyperelastic (compressible Mooney–Rivlin). It should be interesting to extend this optimization approach to elastoplastic materials undergoing large deformations. Finally, the present investigation was confined to the analysis of two-dimensional composites. It should be possible to generalize this micromechanical analysis to a three-dimensional one, thus enabling the study of the behavior of particle filled composites such as rubbery polymers filled with metallic inclusions. In addition, the behavior of metallic foams with open or closed cells can be predicted by employing such a three-dimensional generalization.

References

- [Aboudi 2002] J. Aboudi, “Micromechanical analysis of the fully coupled finite thermoelastic response of rubber-like matrix composites”, *Int. J. Solids Struct.* **39** (2002), 2587–2612.
- [Aboudi 2003] J. Aboudi, “Micromechanical analysis of the finite elastic-viscoplastic response of multiphase composites”, *Int. J. Solids Struct.* **40** (2003), 2793–2817.
- [Aboudi 2004a] J. Aboudi, “Micromechanics-based thermoviscoelastic constitutive equations for rubber-like matrix composites at finite strains”, *Int. J. Solids Struct.* **41** (2004), 5611–5629.
- [Aboudi 2004b] J. Aboudi, “The generalized method of cells and High-fidelity generalized method of cells micromechanical models - a review”, *Mech. Adv. Materl. Struct.* **11** (2004), 329–366.
- [Aboudi and Pindera 2004] J. Aboudi and M.-J. Pindera, “High-fidelity micromechanical modeling of continuously reinforced elastic multiphase materials undergoing finite deformations”, *Math. Mech. Solids* **9:6** (2004), 599–628.
- [Alderson and Alderson 2007] A. Alderson and K. L. Alderson, “Auxetic materials”, pp. 565–575 in *Proc. I. Mech E, Part G: J. Aerospace Eng.*, vol. 221, 2007.
- [Bruck et al. 2007] H. A. Bruck, R. Gilat, J. Aboudi, and A. L. Gershon, “A new approach for optimizing the mechanical behavior of porous microstructures for porous materials by design”, *Modelling Simul. Mater. Sci. Eng.* **15** (2007), 653–674.
- [Gasser and Holzapfel 2002] T. C. Gasser and G. A. Holzapfel, “A rate-independent elastoplastic constitutive model for biological fiber-reinforced composites at finite strains: continuum basis, algorithmic formulation and finite element implementation”, *Comp. Mech.* **29** (2002), 340–360.
- [Hashin and Rosen 1964] Z. Hashin and B. W. Rosen, “The elastic moduli of fiber-reinforced materials”, *J. Appl. Mech.* **31** (1964), 223–232.
- [Herakovich 1998] C. T. Herakovich, *Mechanics of fibrous composites*, Wiley, New York, 1998.
- [Holzapfel 2000] G. A. Holzapfel, *Nonlinear solid mechanics*, John Wiley & Sons Ltd., Chichester, 2000. A continuum approach for engineering.
- [Horgan 1995] C. O. Horgan, “On axisymmetric solutions for compressible nonlinearly elastic solids”, *Z. Angew. Math. Phys.* **46:Special Issue** (1995), S107–S125. Theoretical, experimental, and numerical contributions to the mechanics of fluids and solids.
- [Horgan 2001] C. O. Horgan, “Equilibrium solutions for compressible nonlinearly elastic materials”, pp. 135–159 in *Nonlinear elasticity: theory and applications*, London Math. Soc. Lecture Note Ser. **283**, Cambridge Univ. Press, Cambridge, 2001.
- [Lubliner 1990] J. Lubliner, *Plasticity theory*, Macmillan, New York, 1990.
- [Parton and Kudryavtsev 1993] V. Z. Parton and B. A. Kudryavtsev, *Engineering mechanics of composite structures*, CRC Press, Boca Raton, FL, 1993.
- [Peric 1992] D. Peric, “On consistent stress rates in solid mechanics: computational implications”, *Int. J. Num. Meth. Eng.* **33** (1992), 799–817.
- [Perzyna 1966] P. Perzyna, “Fundamental problems in viscoplasticity”, pp. 243–377 in *Advances in Applied Mechanics*, vol. 9, Academic Press, New York, 1966.
- [Roberts and Shipman 1972] S. M. Roberts and J. S. Shipman, *Two-point boundary value problems: shooting methods*, Modern Analytic and Computational Methods in Science and Mathematics **31**, Elsevier, New York, 1972.

- [Rubin 1987] M. B. Rubin, “An elastic-viscoplastic model exhibiting continuity of solid and liquid states”, *Int. J. Eng. Sci.* **25** (1987), 1175–1191.
- [Simo 1988a] J. C. Simo, “A framework for finite strain elastoplasticity based on maximum plastic dissipation and the multiplicative decomposition. I. Continuum formulation”, *Comput. Methods Appl. Mech. Engrg.* **66:2** (1988), 199–219.
- [Simo 1988b] J. C. Simo, “A framework for finite strain elastoplasticity based on maximum plastic dissipation and the multiplicative decomposition: Part II, computational aspects”, *Comput. Meth. Appl. Mech. Eng.* **68** (1988), 1–31.
- [Simo and Hughes 1998] J. C. Simo and T. J. R. Hughes, *Computational inelasticity*, Interdisciplinary Applied Mathematics **7**, Springer, New York, 1998.
- [van der Sluis et al. 2001] O. van der Sluis, P. J. G. Schreurs, and H. E. H. Meijer, “Homogenisation of structured elasticviscoplastic solids at finite strains”, *Mech. Mater.* **33** (2001), 499–522.
- [Spencer 1971] A. J. M. Spencer, “Theory of invariants”, pp. 239–353 in *Continuum physics*, vol. 1, edited by A. C. Eringen, Academic Press, New York, 1971.
- [Spencer 1984] A. J. Spencer, “Constitutive theory for strongly anisotropic solids”, pp. 1–32 in *Continuum Theory of the Mechanics of Fibre-Reinforced Composites*, vol. 282, edited by A. J. Spencer, Springer-Verlag, Wien, 1984. CISM Courses and Lectures.
- [Surucu et al. 2005] M. Surucu, D. Einstein, and I. Vesely, “Micromechanical modeling of nonlinear viscoelastic behavior of mitral valve chordae”, pp. 924 in *ISB XXth Congress - ASB 29th Annual Meeting*, Cleveland, Ohio, 2005.
- [Tanaka and Yamada 1990] E. Tanaka and H. Yamada, “An inelastic constitutive model of blood vessels”, *Acta Mech.* **82** (1990), 21–30.
- [Tanaka et al. 1996] E. Tanaka, H. Yamada, and S. Murakami, “Inelastic constitutive modeling of arterial and ventricular walls”, pp. 137–163 in *Computational Biomechanics*, edited by K. Hayashi and H. Ishikawa, 1996.

Received 4 Dec 2007. Revised 29 Mar 2008. Accepted 7 Apr 2008.

JACOB ABOUDI: aboudi@eng.tau.ac.il

Faculty of Engineering, Tel Aviv University, Ramat Aviv 69978, Israel

<http://www.eng.tau.ac.il/~aboudi/>